JACS
JOURNAL OF THE AMERICAN CHEMICAL SOCIETY
Article
pubs.acs.org/JACS

Origins of 1,6-Stereoinduction in Torquoselective 6π Electrocyclizations

Ashay Patel,[†] Gregg A. Barcan,[†,‡] Ohyun Kwon,* and K. N. Houk*

Department of Chemistry and Biochemistry, University of California, Los Angeles, California 90095-1234, United States

Supporting Information

ABSTRACT: A novel stereoselective electrocyclization developed for the total synthesis of reserpine has been explored by both experiment and theory. A stereocenter six atoms away from the newly forming chiral center is responsible for the diastereoselectivity of the ring closure. This stereogenic center, lying at the junction of two six-membered rings, defines the conformation of the substrates' fused ring skeleton that ultimately distinguishes between the two allowed, disrotatory triene geometries at the transition state. The presence of allylic strain in the disfavored transition state results in a torquoselective ring closure (dr up to 15.7:1).

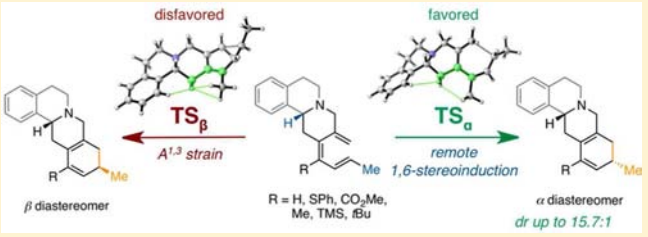

INTRODUCTION

The 6π electrocyclizations of hexatrienes were an impetus for the formulation of the ground-breaking orbital symmetry rules formulated by Woodward and Hoffmann.[1] The orbital symmetry rules predict that the thermal 6π electrocyclization is disrotatory, while the photochemical process is conrotatory (Scheme 1).[2]

Scheme 1. Disrotatory and Conrotatory Modes for the Electrocyclic Ring Closure of 1,3,5-Hexatriene

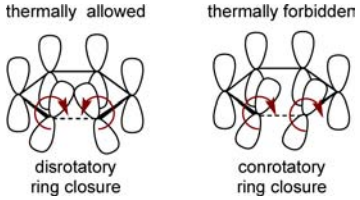

Two modes of disrotation exist for all thermal 6π electrocyclizations. For a chiral substrate, these two disrotatory modes of electrocyclization yield diastereomeric products. If one diastereomer is formed preferentially, such a ring closure is said to be torquoselective (Scheme 2).[3,4]

While the orbital symmetry rules clearly explain that thermal 6π electrocyclizations must occur through disrotation, it is less clear what specific factors control the preference for one disrotatory mode of 6π electrocyclic ring closure over the other. Examples of the torquoselective thermal 6π electrocyclization of hexatrienes date back to 1963,[5] and many examples have been reported since then.[6−15] However, the origins of stereoselectivities in these examples remain unclear.

We recently reported an approach to the reserpine alkaloids based upon a highly torquoselective thermal 6π electrocyclization.[16] Pentacyclic structures were prepared with extremely high levels of selectivity by employing a tandem

Scheme 2. Two Disrotatory Modes of Electrocyclization of a Chiral Hexatriene

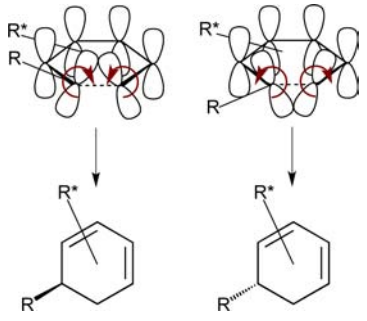

cross-coupling/electrocyclization protocol that relied on a remote stereocenter to induce a diastereoselective ring closure (Scheme 3). Intrigued by the high levels of selectivity observed

Scheme 3. 1,6-Stereoinduction in a 6π Electrocyclization Approach to Reserpine Alkaloids

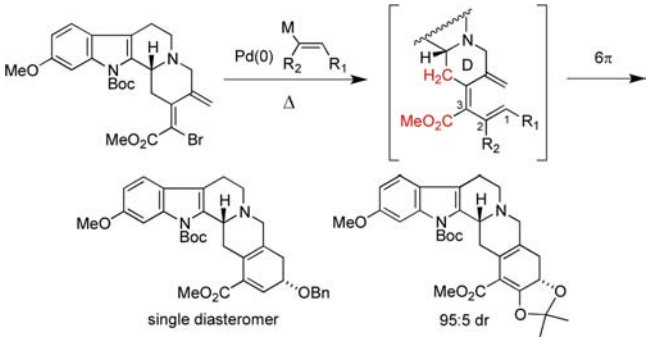

Received: January 28, 2013
Published: February 27, 2013

in these reactions, we explored the scope of this chemistry computationally. Initial results suggested that the methyl ester at the 3-position of the triene could be engaged in allylic strain with the adjacent D-ring methylene. We proposed that varying the steric bulk of groups at the 3-position would have a significant impact on the diastereoselectivity of the electrocyclization. Herein, we report our experimental and computational results investigating the origins of this remote 1,6-stereoinduction.

SYNTHESIS AND ELECTROCYCLIZATION OF TRIENES

In order to assess the effect of substituent size on the electrocyclization reaction, we envisioned an expedient route to several trienes with variations in the size of the functional groups at the 3-position. Our synthetic plan began with the addition of 3-propynylmagnesium bromide to the BF_3-complexed dihydroisoquinoline **1** (Scheme 4).

Scheme 4. Synthesis of Key Enynes 3a–f[a]

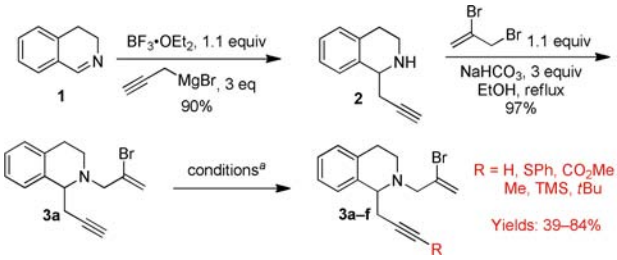

[a]See the Supporting Information for details.

Allylation of amine **2** provided enyne **3a** that was functionalized at the alkyne terminus with groups of varying steric requirement. We then prepared and studied the electrocyclization of six distinct trienes derived from the tandem carbopalladation/cross-coupling of enynes **3a–f** (Table 1).

The tandem carbopalladation/Suzuki coupling sequence generated the corresponding trienes, which upon heating, provided the 6π electrocyclization products. Table 1 provides experimental diastereoselectivities and the A-values of the C3 substituent, as a measure of size, for each triene examined. All of the electrocyclizations took place at 120 °C in xylenes, except for R = CO_2Me and R = TMS that underwent cyclization in the cross-coupling reaction at 80 °C. Starting with the smallest substituent, R = H (Table 1), we observed an increase in the diastereomeric ratio from 3.5:1 to 6.7:1 for R = SPh and then to 15.7:1 and 13.3:1 for R = CO_2Me and R = Me, respectively. The diastereomeric ratio is greater for the reaction of triene **4c**(R = CO_2Me) compared to the ring closure of **4d** (R = Me) due to differences in reaction temperature; however, the experimentally determined $\Delta\Delta G^{\ddagger}$ is larger for the triene **4d** than **4c** (vide infra). The observation that trienes bearing larger substituents provide greater levels of diastereoselectivity than trienes with smaller substitutent is intuitive. Suprisingly, with the larger R = TMS and *R* = *t*Bu substituents, we observe that the diastereomeric ratio decreases to 4.3:1 and 3.2:1, respectively.

COMPUTATIONAL METHODS

All structures examined computationally were initially prepared using Avogadro, a freely available molecular editor/builder program that includes a constrained force field optimization feature useful in generating reasonable starting geometries for QM optimization.[17] Quantum mechanical calculations were performed using Gaussian 09.[18] Geometries were initially optimized in vacuo using the meta-hybrid density functional M06-2X[19] with the 6-31+G(d,p) basis set. Normal-mode analysis confirmed that all optimized reactants and products were indeed minima and that all transition states located were first-order saddle points. Activation barriers ($\Delta H^{\ddagger}$ and $\Delta G^{\ddagger}$) were also determined using M06-2X/def2-TZVPP[20]//M06-2X/6-31+G(d,p) single points with thermal corrections determined at the M06-2X/6-31+G(d,p) level of theory, whereas reaction energies (ΔH_{rxn} and ΔG_{rxn}) were only calculated at the M06-2X/6-31+G(d,p) level of theory. All QM calculations were performed using an "ultrafine" numerical integration grid, consisting of 99 radial shells and 590 angular points per shell. Errors in computed entropies introduced by the treatment of low frequency modes as the harmonic motions

Table 1. Synthesis of Trienes and Experimental Diastereoselectivities of Electrocyclizations

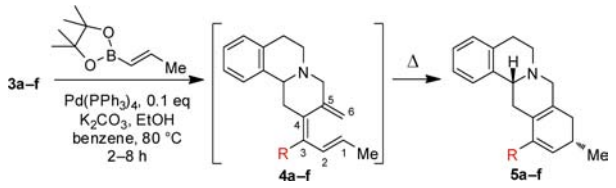

enyne (R)	A-value (kcal/mol)	6π product (dr)[a,b,c]
3a (H)	0	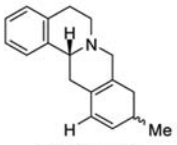 **5a** (3.5:1)
3b (SPh)	0.8	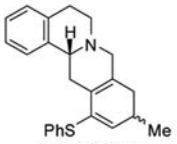 **5b** (6.7:1)
3c (CO_2Me)	1.3	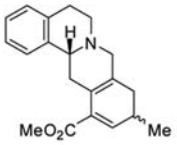 **5c** (15.7:1)
3d (Me)	1.7	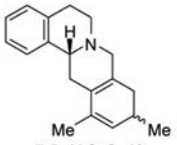 **5d** (13.3:1)
3e (TMS)	2.4	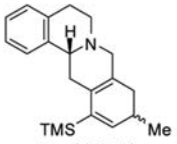 **5c** (4.3:1)
3f (*t*Bu)	>4.5	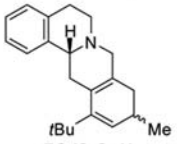 **5f** (3.2:1)

[a]For entries 3 and 5, the electrocyclization product was isolated directly from the cross-coupling reaction without isolation of the triene. All other products were generated by subsequent heating of the isolated triene at 120 °C in xylenes. [b]Diastereomeric ratios determined by ^{1}H NMR. [c]Relative configuration of the new stereogenic center assigned by analogy to a crystal structure of a pentacyclic reserpine precursor (see the Supporting Information).[16]

dx.doi.org/10.1021/ja400882y | J. Am. Chem. Soc. 2013, 135, 4878–4883

were corrected by raising all harmonic frequencies below 100 cm^{-1} to exactly 100 cm^{-1} as described by Truhlar et al.[21] The discussion of stereoselectivity is restricted to only the lowest energy transition-state conformers. A more extensive survey of the structures of transition-state conformers can be found in the Supporting Information.

COMPUTATIONAL RESULTS

The electrocyclizations of trienes **4a–f** (Scheme 5) are all highly exergonic with ΔG_{rxn} values ranging from −18 kcal/mol for the reaction of triene **4a** to −27 kcal/mol for the reaction of triene **4f**. Consequently, the stereoselectivity observed experimentally is due to differences in the energies of the two electrocylicization transition states. The activation energies for this series of electrocyclization reactions are approximately 30 kcal/mol and are consistent with the elevated temperatures required experimentally for the electrocyclization. However, the barriers of the electrocyclic ring closures of trienes **4e** and **4f** are lower ($\Delta G^{\ddagger}$ = 26 kcal/mol) than those for the electrocyclizations of **4a–d**. The computed and experimentally determined energy differences between the lowest energy conformers of the α and β transition states for electrocyclization of **4a–f** are listed in Table 2.

Scheme 5. Six Model Systems Examined Computationally

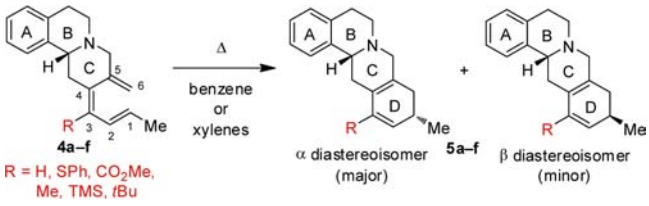

Table 2. A-Values of C3 Substituents, Computed $\Delta\Delta H^{\ddagger}$ and $\Delta\Delta G^{\ddagger}$, and Experimental $\Delta\Delta G^{\ddagger}$ and Values

triene (R)	A-value[a]	comp[b] $\Delta H^{\ddagger}$ ($\Delta G^{\ddagger}$)[a]	comp[b] $\Delta\Delta H^{\ddagger}$ ($\Delta\Delta G^{\ddagger}$)[a]	comp[c] $\Delta\Delta H^{\ddagger}$ ($\Delta\Delta G^{\ddagger}$)[a]	exptl $\Delta\Delta G^{\ddagger}$[a]
4a (H)	0	29.1 (30.2)	0.8 (0.8)	1.0 (1.0)	1.0
4b (SPh)	0.8	28.8 (29.4)	−0.3 (0.1)	0.3 (0.8)	1.5
4c (CO_2Me)	1.2	26.1 (27.2)	1.6 (1.4)	1.6 (1.4)	1.9
4d (Me)	1.7	27.8 (28.8)	2.3 (2.4)	2.4 (2.5)	2.0
4e (TMS)	2.4	25.8 (26.9)	1.2 (1.3)	1.5 (1.6)	1.0
4f (*t*Bu)	>4.5	25.7 (26.8)	−0.2 (−0.7)	−0.1 (−0.7)	0.9

[a]Values in kcal/mol. [b]Gas phase M06-2X/6-31+G(d,p) energies. [c]Gas phase M06-2X/def2-TZVPP//M06-2X/6-31+G(d,p) energies.

In general, computed selectivities for this series of electrocyclic reactions are in reasonable agreement with experimental ones, although we are not able to reproduce the experimental selectivity of the reaction of triene **4f** (R = *t*Bu). As shown in Table 2, computations overestimate the diastereoselectivity of the electrocyclizations of trienes **4d** and **4e** and underestimate the selectivities of the electrocyclic reactions of **4b**, **4c**, and **4f**. The mean absolute deviation (MAD) between the computed $\Delta\Delta G^{\ddagger}$ and corresponding experimental values is 0.6 kcal/mol for this series of electrocyclizations.

For the reactions of **4a**, **4c**, and **4d**, a simple relationship between the steric bulkiness of the C3 substituent, as measured by A-values, and selectivity exists. Triene **4a**, bearing only a hydrogen atom at C3, undergoes ring closure with little diastereoselectivity ($\Delta\Delta G^{\ddagger}$ = 1.0 kcal/mol). Trienes **4c** and **4d** with ester and methyl substituents, respectively, yield more highly selective electrocyclizations ($\Delta\Delta G^{\ddagger}$ = 1.5–2.0 kcal/mol). Despite the relative bulkiness of TMS and *t*Bu, the electrocylizations of trienes **4e** and **4f** are not very selective, according to experiment, and this suggests that the neither the α nor the β transition state can effectively accommodate extremely bulky C3 substituents such as TMS or *t*Bu.

Transition states **TS4d**$_{\alpha}$ and **TS4d**$_{\beta}$ of the electrocyclization of triene **4d** are shown in Figure 2. The triene adopts a boatlike geometry in the disrotatory transition structures, and the two modes of ring closure can be viewed on the right side of Figure 1. In the favored **TS4d**$_{\alpha}$, the C-terminal methyl group rotates downward through a "concave up" boat geometry. The key difference between the two transition states can be found in the dihedral highlighted in green in Figure 1. This dihedral angle is nearly planar (7°) in the disfavored transition structure (**TS4d**$_{\beta}$) and staggered (73°) in the lower-energy **TS4d**$_{\alpha}$. The Newman projections of **TS4d**$_{\alpha}$ and **TS4d**$_{\beta}$ in Figure 2 show more clearly this difference between the two transition

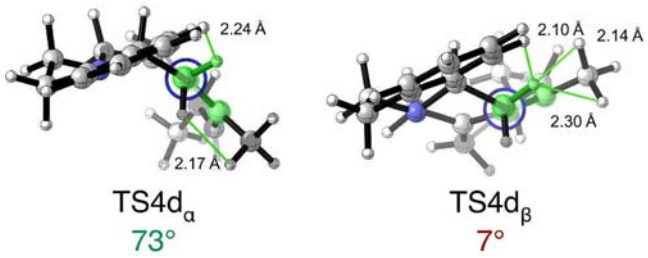

Figure 2. Newman projections of **TS4d**$_{\alpha}$ and **TS4d**$_{\beta}$, highlighting the allylic strain present in the disfavored transition state.

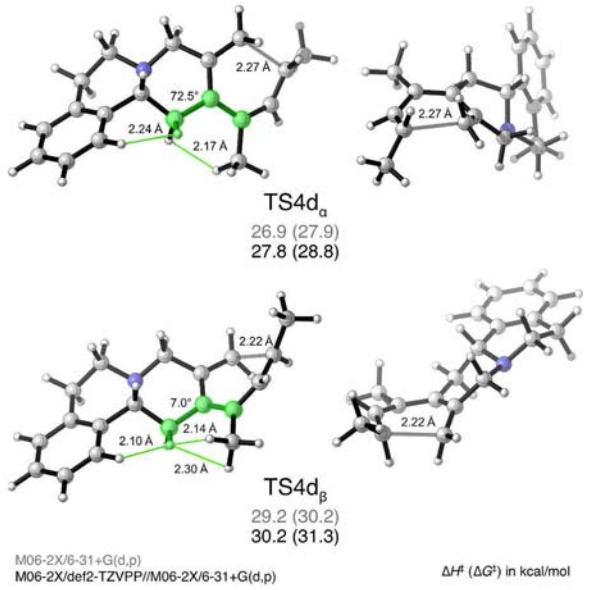

Figure 1. Top and front views of the α and β disrotatory transition states of the electrocyclic reactions of triene **4**, optimized using M06-2X/6-31+G(d,p) in vacuo.

dx.doi.org/10.1021/ja400882y | J. Am. Chem. Soc. 2013, 135, 4878–4883

structures. The planar arrangement in **TS4d**$_\beta$ introduces allylic strain in this transition state between the C3 substitutent and the methylene hydrogen of the piperidine (highlighted). This effect includes contributions from steric clashes between the piperidine hydrogen and the methyl group as well as torsional strain between the two coplanar bonds.

The electrocyclic reactions of tricyclic trienes **4b** and **4f** merit further discussion, as factors beside allylic strain are also important in explaining the torquoselectivity of these ring closures. Triene **4b** possesses a flexible thiophenyl substituent at the C3 position of the triene, introducing the possibility that several rotameric α and β transition states exist. The lowest energy transition-state rotamers leading to the α and β diastereomers, **TS4b**$_\alpha$ and **TS4b**$_\beta$, respectively, are shown in Figure 3. **TS4b**$_\alpha$ is 0.8 kcal/mol lower in free energy than

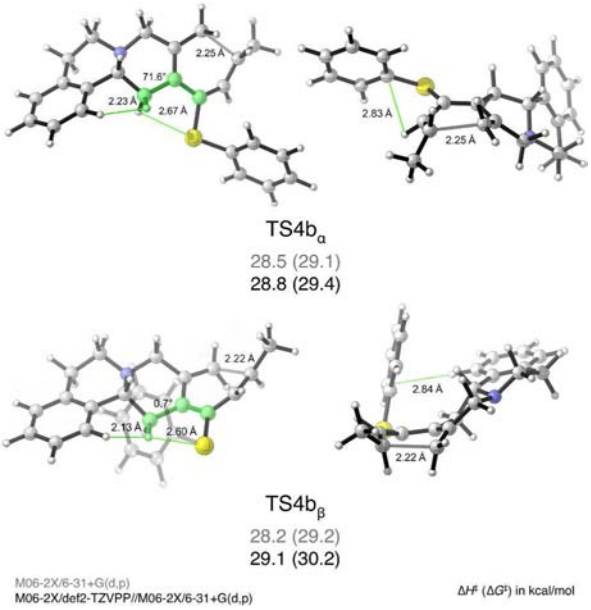

Figure 3. Top and front views of the α and β disrotatory transition states of the electrocyclic reaction of triene **4b** optimized using M06-2X/6-31+G(d,p) in vacuo. Note the *S*-phenyl group is made transparent for clarity where necessary.

TS4b$_\beta$ according to the large basis set calculations. This $\Delta\Delta G^{\ddagger}$ value is smaller than the 1.5 kcal/mol value observed experimentally. The difference in the corresponding H−C−C−C dihedral between **TS4b**$_\alpha$ and **TS4b**$_\beta$ is even larger than that of **TS4d**$_\alpha$ and **TS4d**$_\beta$, as the dihedral angle in **TS4b**$_\beta$ is 0.7° presumably because the thiophenyl substituent is conjugated with the triene in this structure. Allylic strain in **TS4b**$_\beta$ may be attenuated by electrostatic attraction between the electronegative sulfur atom and the positively charged hydrogen atom; however, torsional strain will still destabilize **TS4b**$_\beta$ relative to **TS4b**$_\alpha$.

TS4b$_\alpha$ and **TS4b**$_\beta$ are both stabilized by intramolecular C−H π interactions that could provide stabilization by dispersion. In **TS4b**$_\alpha$, the C−H π interaction occurs between the *S*-phenyl group and the C2 hydrogen of the triene (2.85 Å). A similar interaction occurs in **TS4b**$_\beta$ between the *S*-phenyl group and an aromatic hydrogen of the aromatic A-ring (2.84 Å). Because the reactions are performed in xylenes, the solvent may be competing with the *S*-phenyl group for these weak interactions in such way that the two transition states may not be differentially stabilized. In order to estimate the selectivity that would exist in the absence of these intramolecular dispersion interactions, we replaced the phenyl group with a hydrogen atom or methyl group and performed single point energy calculations on these structures. $\Delta\Delta E$ between these model trienes are 5.9 and 4.9 kcal/mol, respectively, favoring the formation of the α diastereomer.

According to computations, the reaction of **4f** proceeds with a $\Delta G^{\ddagger}$ value of 25 kcal/mol and a ΔG_{rxn} value of −27 kcal/mol. These values are similar to corresponding values determined for the reaction of **4e**. In comparison to the electrocyclizations of trienes **4a**−**d**, **4e** and **4f** undergo ring closures with a 3−5 kcal/mol lower barrier and are also 3−7 kcal/mol more exergonic. The diminished barrier and the increased exergonicity of the electrocyclizations of both **4e** and **4f** are due to a decrease in steric demand for the bulky C3 substituent as the reactant progresses along the reaction coordinate toward the product. Computations also indicate that the electrocyclic reaction of triene **4f** (R = *t*Bu) is essentially nonselective, with a slight preference for the β stereoisomer (minor product). Illustrated in Figure 4 are the α and β transition states for this

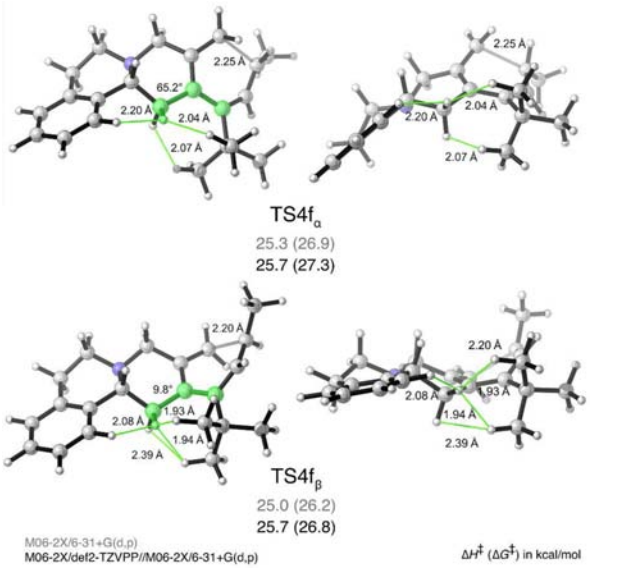

Figure 4. Top and back views of the α and β disrotatory transition states of the electrocyclic reaction of triene **4d** optimized using M06-2X/6-31+G(d,p) in vacuo.

electrocyclization. Both **TS4f**$_\alpha$ and **TS4f**$_\beta$ suffer from a number of steric clashes, some of which are quite severe and range in terms of interatomic (H−H) distances from 1.94 to 2.07 Å. The introduction of additional steric clashes in the α transition state of **4f** leads to the erosion of selectivity observed experimentally.

■ ORIGINS OF DIFFERENTIAL ALLYLIC STRAIN IN THE ELECTROCYCLIZATION TRANSITION STATES OF TRIENES 4A−F

The piperidine ring (C-ring, Scheme 5) directly fused to the triene discriminates between the two modes of disrotation. This ring prefers to adopt a half-chair conformation, which places the hydrogen at the stereocenter in an axial position. Overlaying the piperidine rings (heavy atoms only) of the α and β transition structures (**TS4**$_\alpha$ and **TS4**$_\beta$) reveals the conformations of this heterocycle in either transition state are nearly identical (RMSD 0.17 Å).

dx.doi.org/10.1021/ja400882y | *J. Am. Chem. Soc.* 2013, 135, 4878−4883

How does this piperidine ring cause the two disrotatory modes to have different energies? In the α transition states, the triene adopts a "concave up" boat geometry. This arrangement places the C3 substituent (see Figures 1 and 2) between the pseudoaxial and pseudoequatorial hydrogens of the piperidine ring. Eclipsing strain is avoided as the C3−C4 bond of the triene also lies between these hydrogens. In the β transition states, the triene features a "concave down" boat that forces the C3−C4 bond into the plane of the pseudoequatorial C−H bond (Figures 1 and 2), introducing eclipsing strain as well as allylic strain between the C3 substituent and the pseudoequatorial hydrogen.

Remote stereoinduction in this manifold is only possible because the triene adopts one of two well-defined, clearly distinguishable boatlike geometries (i.e., "concave up" or "concave down") at the transition state. These boatlike transition states have rigid geometries that do not distort easily, since the boat arrangement of the triene maximizes orbital overlap[22] within the cyclic array of p orbitals, while conforming to the rules of orbital symmetry. Overlays of the triene portions of **TS4a$_\beta$**−**TS4f$_\beta$** confirm this recalcitrance toward distortion as the triene geometries are conserved throughout the series of trienes, even for **TS4e$_\beta$** (R = TMS) and **TS4f$_\beta$** (R = *t*Bu).

CONCLUSIONS

We have explored the torquoselective 6π electrocyclizations of a series of isoquinoline-derived trienes differentially functionalized at the 3-position of the triene experimentally and computationally. For the six trienes examined, there is a qualitative agreement between theory and experiment. The observed diastereoselectivities for this series of triene electrocyclizations are sensitive to substitution at the C3 position of the triene. Trienes bearing moderately bulky substituents such as methyl or methyl ester at this position undergo 6π electrocyclization with the greatest levels of diastereoselectivity, whereas trienes with more bulky C3 substituents such as R = TMS or R = *t*Bu undergo a much less stereoselective ring closure. Our results also illustrate that the conformation of the piperidine ring (C-ring) in conjunction with the strict geometric requirements of the triene at the transition state are responsible for the relay of stereochemical information from a distal stereogenic center to the forming stereocenter six atoms away. Allylic strain in the β transition states explains the observed preference for the α diastereomer in this series of electrocyclizations.

ASSOCIATED CONTENT

Supporting Information

Relevant NMR data, synthetic details, coordinates for computed structures in *xyz* format, details regarding the conformational analysis of the transition states, and computational methods. This material is available free of charge via the Internet at http://pubs.acs.org.

AUTHOR INFORMATION

Corresponding Author

houk@chem.ucla.edu; ohyun@chem.ucla.edu

Present Address

[‡]Gregg A. Barcan: Department of Chemistry, Stanford University, Stanford, California, 94305-5080, United States.

Author Contributions

[†]These authors contributed equally.

Notes

The authors declare no competing financial interests.

ACKNOWLEDGMENTS

A.P. and K.N.H. acknowledge the financial support of the NIH (GM-36700 to K.N.H.). A.P. thanks the Chemical-Biology Interface Training Program for its support (T32 GM 008496). The following computational resources were used in this study: the Hoffman2 cluster at UCLA and the Extreme Science and Engineering Discovery Environment (XSEDE) supported by the NSF (OCI-1053575). O.K. and G.A.B. acknowledge funding from the NIH (R01GM071779) and the NSF (equipment grant CHE-1048804).

REFERENCES

(1) Woodward, R. B.; Hoffmann, R. *J. Am. Chem. Soc.* **1965**, *87*, 395−397.
(2) Woodward, R. B.; Hoffmann, R. *Angew. Chem., Int. Ed.* **1969**, *8*, 781−932.
(3) Rondan, N. G.; Houk, K. N. *J. Am. Chem. Soc.* **1985**, *107*, 2099−2111.
(4) Kirmse, W.; Rondan, N. G.; Houk, K. N. *J. Am. Chem. Soc.* **1984**, *106*, 7989−7991.
(5) Corey, E. J.; Hortmann, A. G. *J. Am. Chem. Soc.* **1963**, *85*, 4033−4034.
(6) Okamura, W. H.; Peter, R.; Reischl, W. *J. Am. Chem. Soc.* **1985**, *107*, 1034−1041.
(7) Bamba, M.; Nishikawa, T.; Isobe, M. *Tetrahedron Lett.* **1996**, *37*, 8199−8202.
(8) Bamba, M.; Nishikawa, T.; Isobe, M. *Tetrahedron* **1998**, *54*, 6639−6650.
(9) Whitesell, J. K.; Minton, M. A. *J. Am. Chem. Soc.* **1987**, *109*, 6403−6408.
(10) Benson, C. L.; West, F. G. *Org. Lett.* **2007**, *9*, 2545−2548.
(11) Jung, M. E.; Min, S.-J. *Tetrahedron* **2007**, *63*, 3682−3701.
(12) Hayashi, R.; Feltenberger, J. B.; Hsung, R. P. *Org. Lett.* **2010**, *12*, 1152−1155.
(13) Hayashi, R.; Walton, M. C.; Hsung, R. P.; Schwab, J. H.; Yu, X. *Org. Lett.* **2010**, *12*, 5768−5771.
(14) Katsunori, T.; Katsumura, S. *J. Am. Chem. Soc.* **2002**, *124*, 9660−9661.
(15) Sklenicka, H. M.; Hsung, R. P.; McLaughlin, M. J.; Wei, L.-L.; Gerasyuto, A. I.; Brennessel, W. B. *J. Am. Chem. Soc.* **2002**, *124*, 10435−10442.
(16) Barcan, G. A.; Patel, A.; Houk, K. N.; Kwon, O. *Org. Lett.* **2012**, *14*, 5388−5391.
(17) Hanwell, M. D.; Curtis, D. E.; Lonie, D. C.; Vandermeersch, T.; Zurek, E.; Hutchison, G. R. *J. Cheminf.* **2012**, *4*, 17.
(18) Frisch, M. J.; Trucks, G. W.; Schlegel, H. B.; Scuseria, G. E.; Robb, M. A.; Cheeseman, J. R.; Scalmani, G.; Barone, V.; Mennucci, B.; Petersson, G. A.; Nakatsuji, H.; Caricato, M.; Li, X.; Hratchian, H. P.; Izmaylov, A. F.; Bloino, J.; Zheng, G.; Sonnenberg, J. L.; Hada, M.; Ehara, M.; Toyota, K.; Fukuda, R.; Hasegawa, J.; Ishida, M.; Nakajima, T.; Honda, Y.; Kitao, O.; Nakai, H.; Vreven, T.; Montgomery, J. A.; Peralta, J. E.; Ogliaro, F.; Bearpark, M.; Heyd, J. J.; Brothers, E.; Kudin, K. N.; Staroverov, V. N.; Kobayashi, R.; Normand, J.; Raghavachari, K.; Rendell, A.; Burant, J. C.; Iyengar, S. S.; Tomasi, J.; Cossi, M.; Rega, N.; Millam, J. M.; Klene, M.; Knox, J. E.; Cross, J. B.; Bakken, V.; Adamo, C.; Jaramillo, J.; Gomperts, R.; Stratmann, R. E.; Yazyev, O.; Austin, A. J.; Cammi, R.; Pomelli, C.; Ochterski, J. W.; Martin, R. L.; Morokuma, K.; Zakrzewski, V. G.; Voth, G. A.; Salvador, P.; Dannenberg, J. J.; Dapprich, S.; Daniels, A. D.; Farkas, O.; Foresman, J. B.; Ortiz, J. V.; Cioslowski, J.; Fox, D. J. *Gaussian 09*, revision C.01; Gaussian, Inc.: Wallingford, CT, 2009.
(19) Zhao, Y.; Truhlar, D. *Theor. Chem. Acc.* **2008**, *120*, 215−241.

(20) Weigend, F.; Ahlrichs, R. *Phys. Chem. Chem. Phys.* **2005**, *7*, 3297−3305.
(21) Ribeiro, R. F.; Marenich, A. V.; Cramer, C. J.; Truhlar, D. G. *J. Phys. Chem. B* **2011**, *115*, 14556−14562.
(22) Houk, K. N.; Li, Y.; Evanseck, J. D. *Angew. Chem., Int. Ed. Engl.* **1992**, *31*, 682−708.